Electronic Supplementary Information

A Heterostructured FeNi Hydroxide for Effective Electrocatalytic Oxygen Evolution

Fayan Li,[a] Yanyan Li,[a] Lei Li,[a] Wen Luo,[b] Zhouguang Lu,[b] Xinyu Zhang,[a,] and Zhiping Zheng[a,*]*

[a] Department of Chemistry, Guangdong Provincial Key Laboratory of Energy Materials for Electric Power, Southern University of Science and Technology (SUSTech), Shenzhen 518055, China; Key Laboratory of Energy Conversion and Storage Technologies (SUSTech), Ministry of Education, Shenzhen 518055, China

[b] Department of Materials Science and Engineering, SUSTech, Shenzhen 518055, China

*Corresponding Authors: Xinyu Zhang (zhangx1@sustech.edu.cn), Zhiping Zheng (zhengzp@sustech.edu.cn)

Contents

1. Experimental Procedures

1.1. Materials

$FeCl_3·6H_2O$ (≥ 99.0%, Shanghai Titan Scientific Co., Ltd.), $NiCl_2·6H_2O$ (≥ 99.0%, Shanghai Titan Scientific Co., Ltd.), $CoCl_2·6H_2O$ (≥ 99.0%, Shanghai Titan Scientific Co., Ltd.), gelatin ($C_{102}H_{151}N_{31}O_{39}$, G7041-500G, Sigma-Aldrich), urea ($CO(NH_2)_2$, 99.0%, Shanghai Titan Scientific Co., Ltd.) were used as received without further purification. Deionized (DI) water was used in all experiments.

1.2. Synthesis

1.2.1 Synthesis of FeNi/Ni HS

A solution was prepared by dissolving $FeCl_3·6H_2O$ (2.16 g, 8 mmol) and $NiCl_2·6H_2O$ (2.85 g, 12 mmol) in 40 mL of DI water with sonication, to which an aqueous solution of gelatin (8 mL) was prepared by dissolving 1 g of gelatin in 9 mL of DI water at 85 ℃) was slowly added over 15 min with sonication, followed by the addition of 8 g of urea. The resulting mixture was sonicated for another 20 min till a clear solution was obtained. The reaction continued at 100 ℃ for 36 h. The reaction mixture was then cooled to room temperature and then centrifuged at 8000 rpm for 5 min. The precipitate was collected and washed with absolute ethanol and DI water three times and dried at 60 ℃ in a vacuum oven.

1.2.2. Synthesis of FeOOH

The synthetic procedure of FeOOH was similar to that of FeNi/Ni HS, except that with the use of $FeCl_3·6H_2O$ (2.70 g, 10 mmol), DI water (20 mL), and urea (3 g).

1.2.3. Synthesis of $Ni_2(CO_3)(OH)_2$

The synthetic procedure of $Ni_2(CO_3)(OH)_2$ was similar to that of FeNi/Ni HS, except that with the use of $NiCl_2·6H_2O$ (2.38 g, 10 mmol), DI water (20 mL), and urea (3 g).

1.2.4. Synthesis of the Physical Mixture of FeOOH and $Ni_2(CO_3)(OH)_2$

The physical mixture was prepared by mixing FeOOH (0.71 g, 8 mmol) and $Ni_2(CO_3)(OH)_2$ (1.27 g, 6 mmol).

1.2.5. Synthesis of Ni-doped FeOOH

Ni-doped FeOOH was obtained by reacting according to the synthesis conditions of FeNi/Ni HS for 3h.

1.2.6. Synthesis of $Co(CO_3)_{0.5}(OH)$

The synthetic procedure of $Co(CO_3)_{0.5}(OH)$ was similar to that of FeNi/Ni HS, except that with the use of $CoCl_2 \cdot 6H_2O$ (2.38 g, 10 mmol), DI water (20 mL), and urea (3 g).

1.2.7. Synthesis of the Physical Mixture of FeOOH and $Co(CO_3)_{0.5}(OH)$

The physical mixture was prepared by mixing FeOOH (0.89 g, 10 mmol) and $Co(CO_3)_{0.5}(OH)$ (1.06 g, 10 mmol).

1.2.8. Synthesis of Co-doped FeOOH

Co-doped FeOOH was obtained by reacting according to the synthesis conditions of FeNi/Ni HS for 3h.

1.2.9. Synthesis of FeCo/Co HS

The synthetic procedure of FeCo/Co HS was similar to that of FeNi/Ni HS, except that with a mixture of $FeCl_3 \cdot 6H_2O$ (2.70 g, 10 mmol) and $CoCl_2 \cdot 6H_2O$ (2.38 g, 10 mmol).

1.3. Characterization

The field emission scanning electron microscopy (SEM) images were taken on a Merlin scanning electron microscopy with an accelerating voltage of 5 kV. Transmission electron microscope (TEM) images were acquired on a Hitachi HT-7700 (Japan) transmission electron microscope with an accelerating voltage of 100 kV. Atomic-resolution high-angle annular dark field-scanning transmission electron microscopy (HAADF-STEM) images, energy-dispersive X-

ray spectroscopy (EDX), and electron energy loss spectroscopy (EELS) characterizations were performed with a Titan Themis G2 operating at 300 kV.

X-ray diffraction (XRD) patterns of the dried samples were measured in a Rigaku D/MAX-RB (Japan) X-ray diffractometer with Cu-Kα radiation (*λ*=1.5406 Å). X-ray photoelectron spectroscopy (XPS) was recorded on a PHI 5000 Versa Probe III with Al Kα (hν=1486.6 eV) as the excitation source. With reference to C 1s to 284.6 eV, the binding energy obtained in XPS spectra analysis was corrected. Raman spectra of powder samples were recorded on a Renishaw Invia Raman Microscope with a laser excitation wavelength of 532 nm. *In-situ* Raman tests for catalysts were conducted in a homemade electrochemical cell under controlled potentials. The concentration of catalysts was determined by inductively coupled plasma mass spectroscopy (ICP-MS) (Agilent 7700x).

1.4. Electrocatalytic Research

1.4.1. Electrocatalytic Measurements

electrochemical measurements of OER performance were performed using the CHI 760E Electrochemical Workstation (rotating disk electrode (RDE), electrode area: 0.07 cm^2) with a standard three-electrode system, the RDE as the working electrode, carbon rode as the counter electrode, and a saturated Ag/AgCl electrode (in saturated KCl solution) as the reference electrode. The potentials values used in this study were calculated according to the following equation: $E\,(\text{vs. RHE}) = E_{\text{Ag/AgCl}} + 0.197\ \text{V} + 0.0591\ \text{pH}$. Overpotentials ($\eta$) were calculated based on the formula $\eta = E\,(\text{vs. RHE}) - 1.23\ \text{V}$. Current density ($j$) was calculated by dividing the current by the electrode area. The working electrode was prepared according to the following methods. Typically, 4 mg of as-prepared catalyst and 1 mg of activated carbon powder were dispersed in 480 μL deionized (DI) water, 480 μL ethanol, and 40 μL Nafion mixture solution. Then the mixture solution was sonicated for 2 h to form a homogeneous ink. After that, 5 μL of the dispersion was loaded onto the RDE. All the loading mass of the

catalysts on the RDE was about 0.028 mg cm^{-2}. Electrocatalytic performances were carried out in 1.0 M KOH. The working electrode was performed with a rotation rate of 1600 rpm. The electrochemical impedance spectroscopy (EIS) measurements were carried out in the same configuration at 1.32 V (vs. RHE) from 0.1 Hz to 100 kHz.

The electrical double layer capacitance (C_{dl}) of the samples was measured from double-layer charging curves using cyclic voltammograms (CVs) in a potential range of 1.02-1.12 V in 1.0 M KOH at the scan rate of 10, 20, 30, 40, 50, 60, 70, and 80 mV s^{-1}.

1.4.2. Calculation of ECSA-normalized Current Density

The electrochemical surface area (ECSA) is estimated from C_{dl} of the catalyst. The ECSA-normalized current density (j_{ECSA}) is calculated as follows:

$$\mathrm{ECSA} = C_{dl}/Cs$$

$$j_{ECSA} = j/\mathrm{ECSA}$$

where *C*s is the specific capacitance (0.04 mF cm^{-2} in this work). While *j* is the current (mA).[1,2]

1.4.3. Calculation of Mass Activity and TOF

The mass activity (A/g) values were calculated from the catalyst loading m (0.28 mg cm^{-2}) and the measured current density *j* (mA cm^{-2}) at $\eta = 268\ \mathrm{mV}$.

$$\text{Mass activity} = j/\mathrm{m}$$

The TOF values were calculated by assuming that every metal atom is involved in the catalysis (lower TOF limits were calculated):

$$\mathrm{TOF} = j\mathrm{S}/4\mathrm{Fn}$$

Where j (mA cm^{-2}) is the measured current density at η=268 mV, S (0.07 cm^2) is the surface area of the glassy carbon electrode, the constant 4 means 4 electrons/mol of O_2, F is Faraday's constant (96485.30 C/mol), and n is the mole of coated metal atom on the electrode calculated from m, the molecular weight of the coated catalysts.

1.4.4. Measurement of the Faradic Efficiency

The Faradic efficiency for OER was determined by a rotating ring-disk electrode (RRDE) consisting of a glassy carbon disk electrode and a Pt ring electrode. A constant current of 200 μA was applied to the disk electrode, and the ring electrode was held constant at 0.40 V *vs* RHE to reduce O_2 generated at the disk. The Faradic efficiency (f) is calculated using the following equation:

$$f = \frac{I_r}{N I_d}$$

Where I_d is the disk current and I_r is the ring current. N is the current collection efficiency of the RRDE (0.2) determined using the same configuration with an IrO_2 thin-film electrode.[3,4]

2. Supporting Figures and Tables

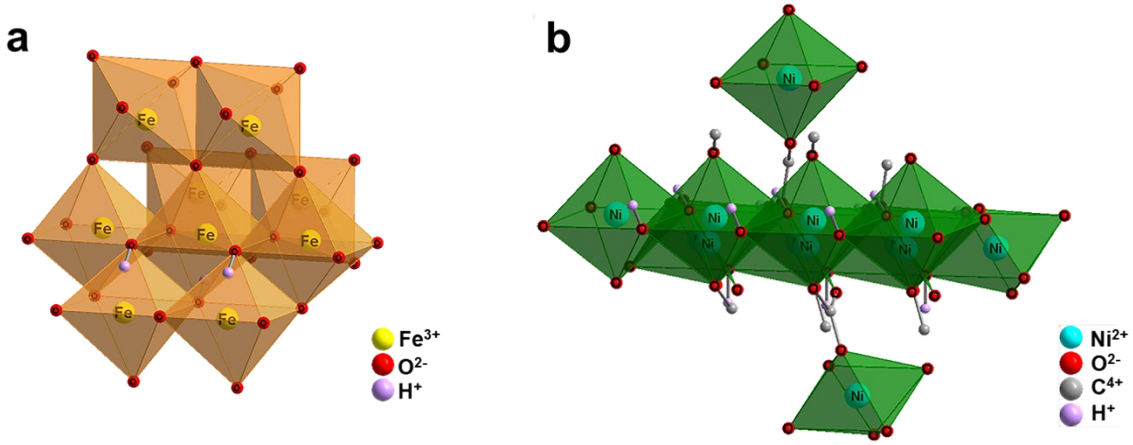

Fig. S1 Crystal structures of (a) FeOOH and (b) $Ni_2(CO_3)(OH)_2$.

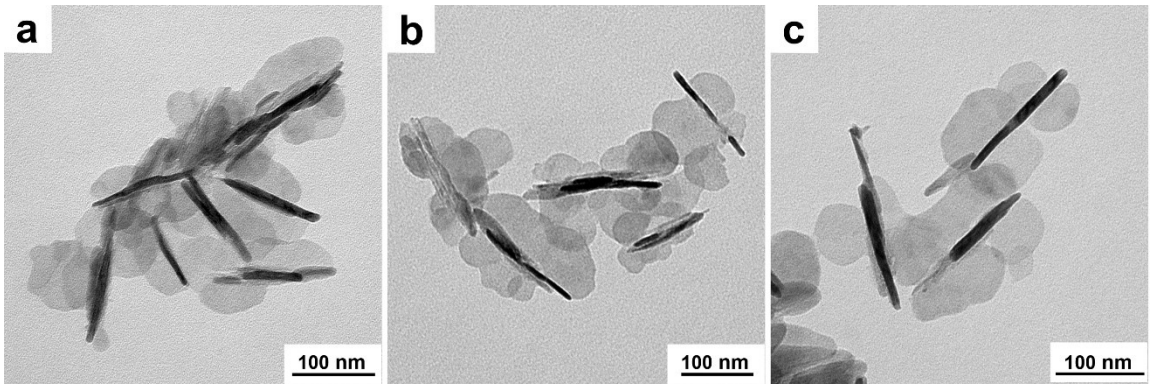

Fig. S2 TEM images of FeNi/Ni HS.

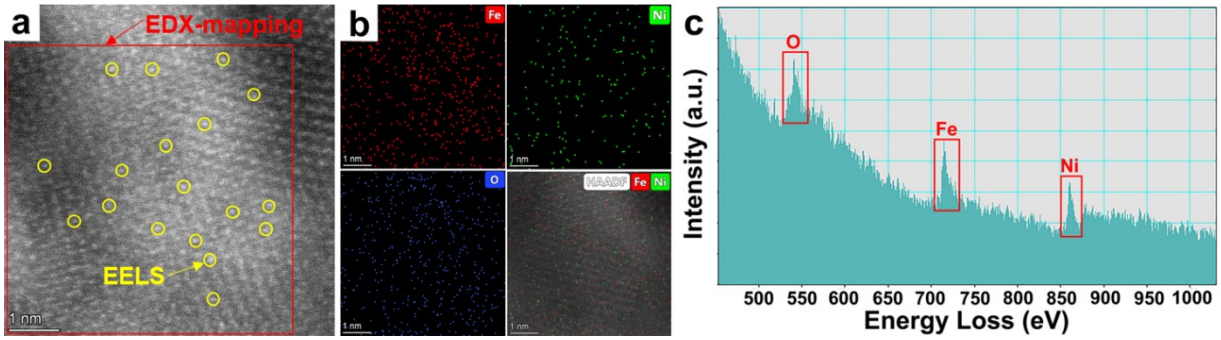

Fig. S3 Cs-corrected HRTEM characterization of the "torso" region: (a) the HAADF-STEM. The red rectangular box is the EDX-mapping collection area, and the yellow circles indicate where the EELS data were collected. (b) the high-resolution EDX-mapping, (c) the spot-scanning EELS. The Fe and O signals are clearly shown in EELS spectrum because FeOOH as substrate is present in a large quantity.

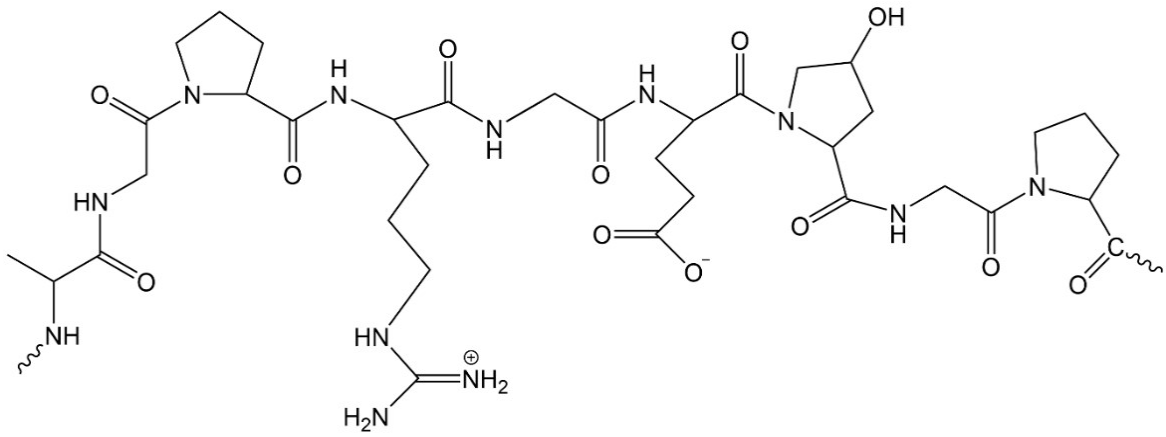

Fig. S4 The basic molecular unit of gelatin.

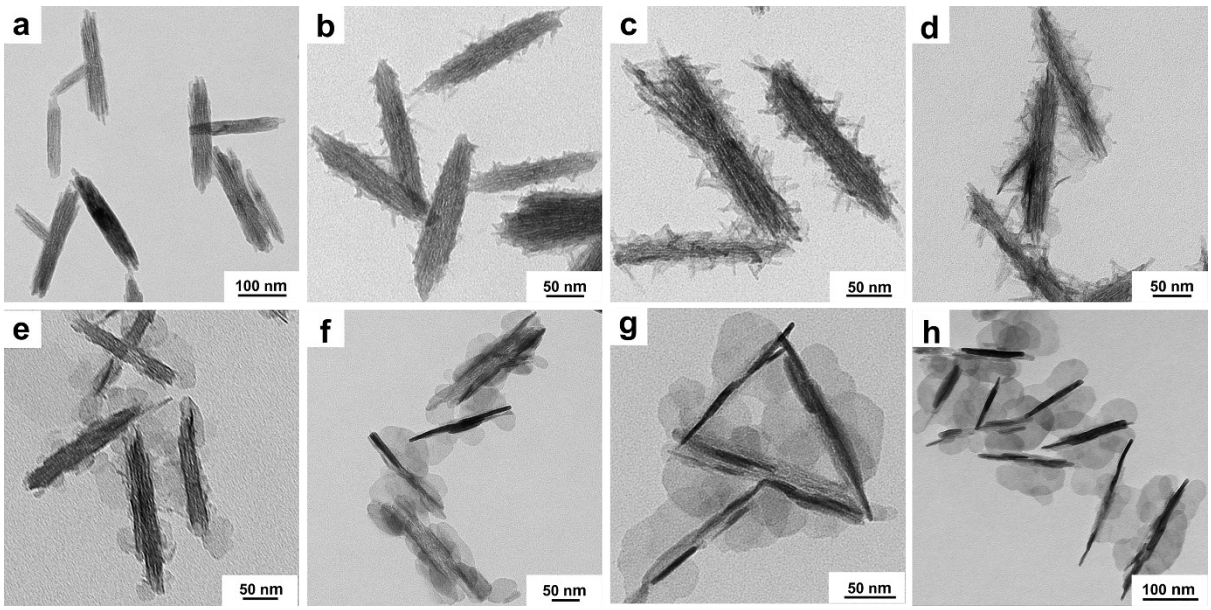

Fig. S5 Growth characteristics of FeNi/Ni HS over a course of 36 h. (a) 3 h, (b) 6 h, (c) 12 h, (d) 18 h, (e) 21 h, (f) 27 h, (g) 33 h, (h) 36 h.

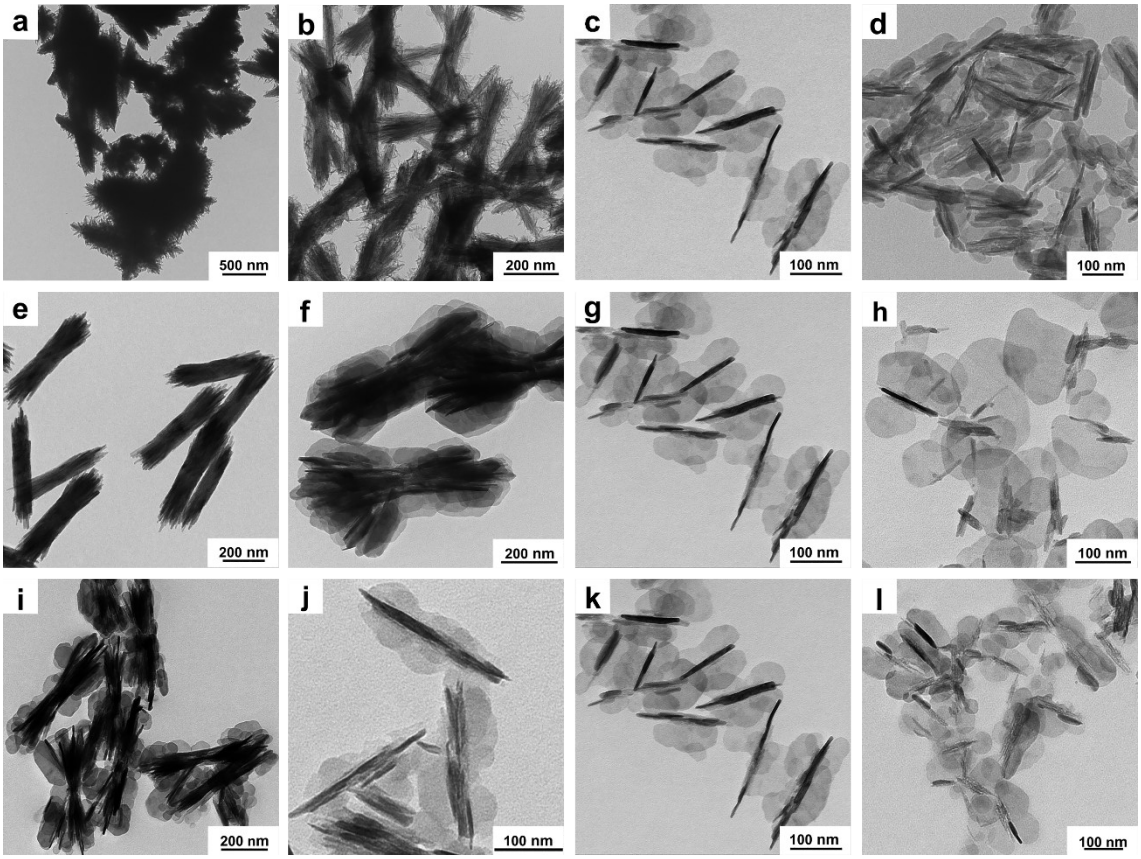

Fig. S6 Other conditions-dependent growth characteristics of FeNi/Ni HS. (a-d) After reaction for 36 h, with different dosages of gelatin (urea=8 g, $NiCl_2 \cdot 6H_2O/FeCl_3 \cdot 6H_2O$=3/2): (a) gelatin=0 mL, (b) gelatin=4 mL, (c) gelatin=8 mL, (d) gelatin=16 mL. (e-h) After reaction for 36 h, with different dosages of urea (gelatin=8 mL, $NiCl_2 \cdot 6H_2O/FeCl_3 \cdot 6H_2O$=3/2): (e) urea=0 g, (f) urea=4 g, (g) urea=8 g, (h) urea=16 g. (i-l) After reaction for 36 h, with different precursor mole ratios (urea=8 g, gelatin=8 mL): (i) $NiCl_2 \cdot 6H_2O/FeCl_3 \cdot 6H_2O$=1/2, (j) $NiCl_2 \cdot 6H_2O/FeCl_3 \cdot 6H_2O$=1/1, (k) $NiCl_2 \cdot 6H_2O/FeCl_3 \cdot 6H_2O$=3/2, (l) $NiCl_2 \cdot 6H_2O/FeCl_3 \cdot 6H_2O$=2/1.

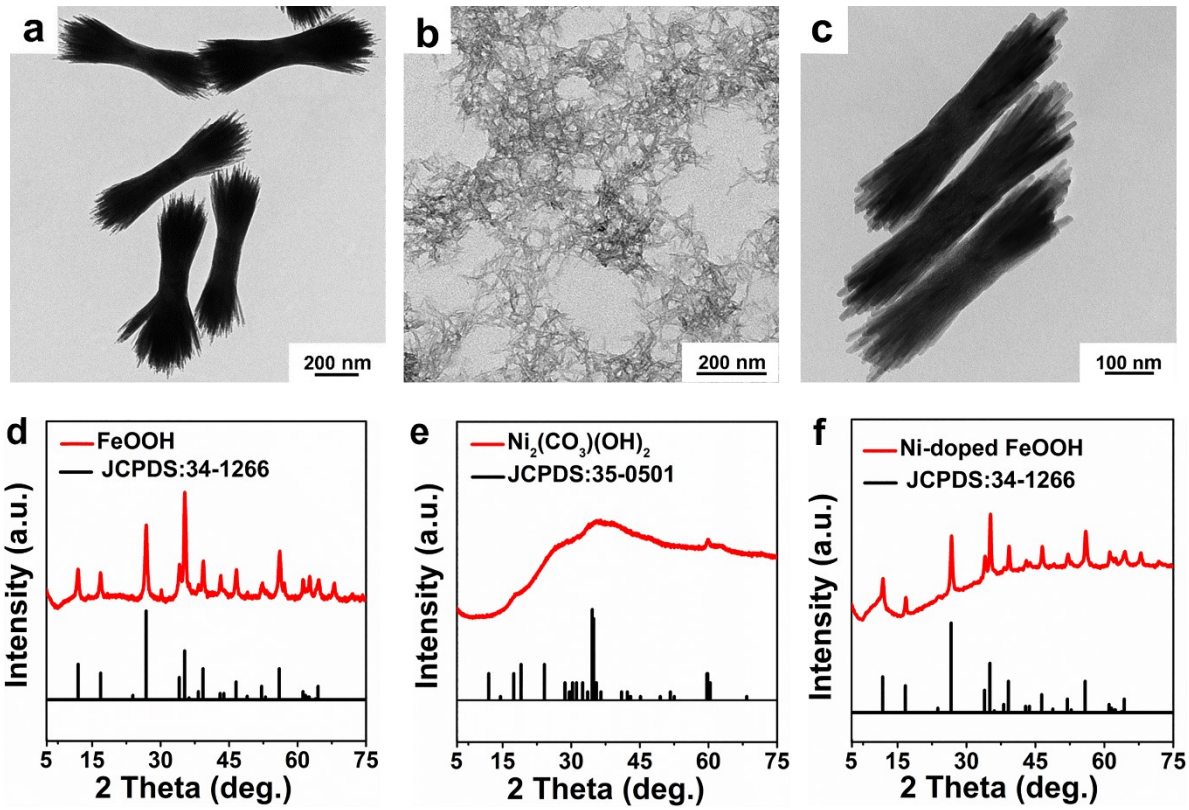

Fig. S7 Morphological and structural characterizations of the compared samples. TEM images of (a) FeOOH, (b) $Ni_2(CO_3)(OH)_2$, and (c) Ni-FeOOH; XRD patterns of (d) FeOOH, (e) $Ni_2(CO_3)(OH)_2$, and (f) Ni-FeOOH.

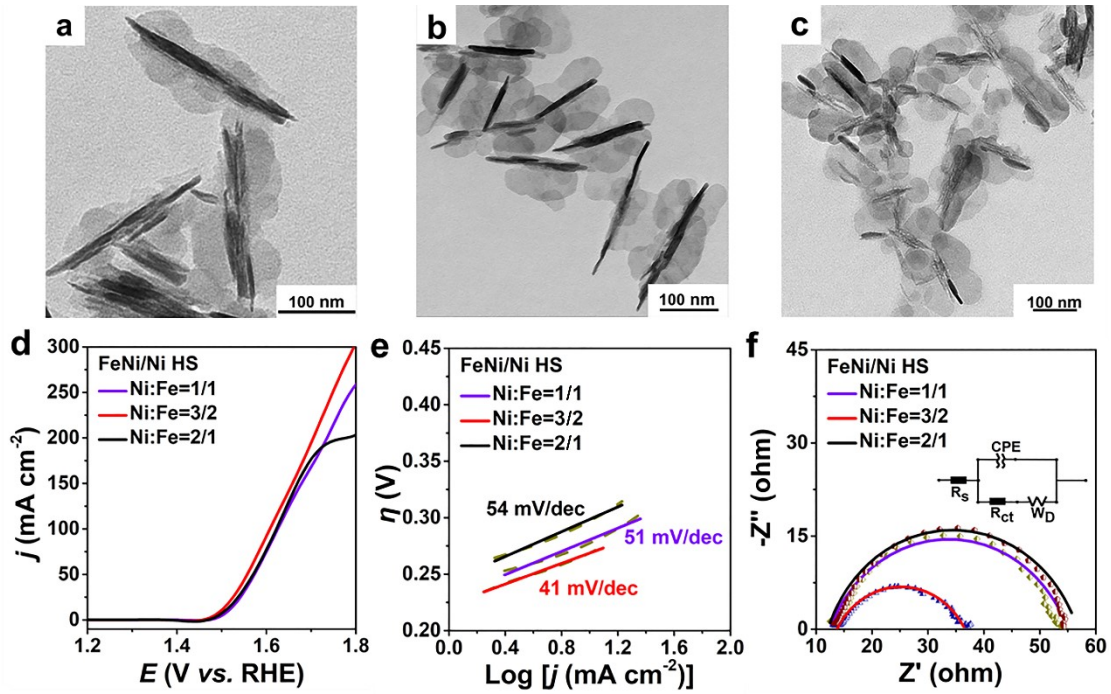

Fig. S8 TEM images of different FeNi/Ni HS more ratios (a) Ni:Fe=1:1, (b) Ni:Fe=3:2, (c) Ni:Fe=2:1. Comparative electrochemical studies: (d) Liner sweep voltammetry (LSV), (e) Tafel plots (log *j* - *η*), (f) Nyquist plots.

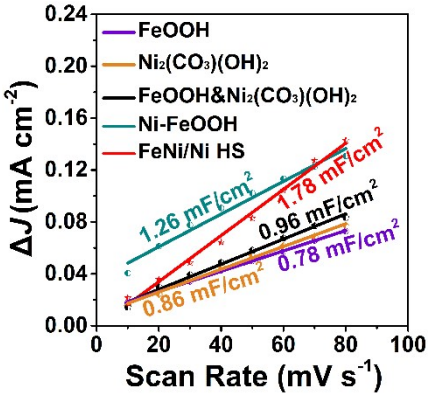

Fig. S9 C_{dl} calculations of catalysts.

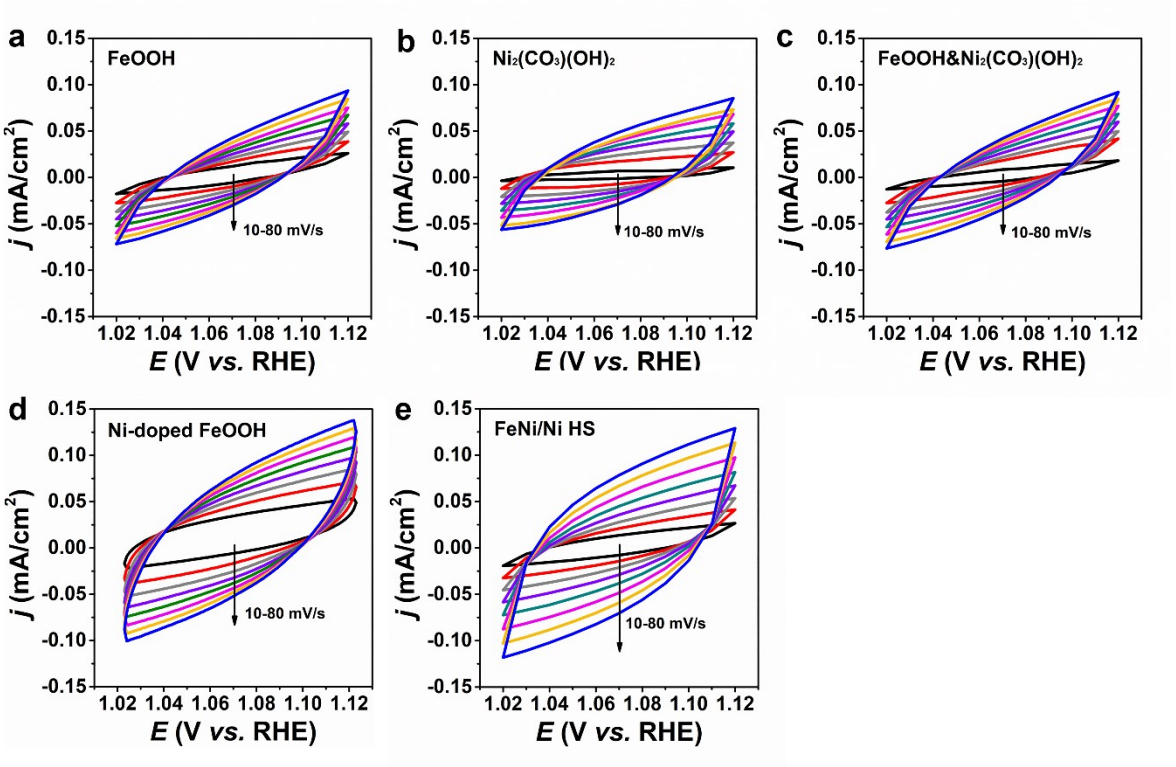

Fig. S10 Typical cyclic voltammetry curves of (a) FeOOH, (b) $Ni_2(CO_3)(OH)_2$, (c) FeOOH&$Ni_2(CO_3)(OH)_2$, (d) Ni-FeOOH and (e) FeNi/Ni HS in 1.0 M KOH with different scan rates (10-80 mV/s).

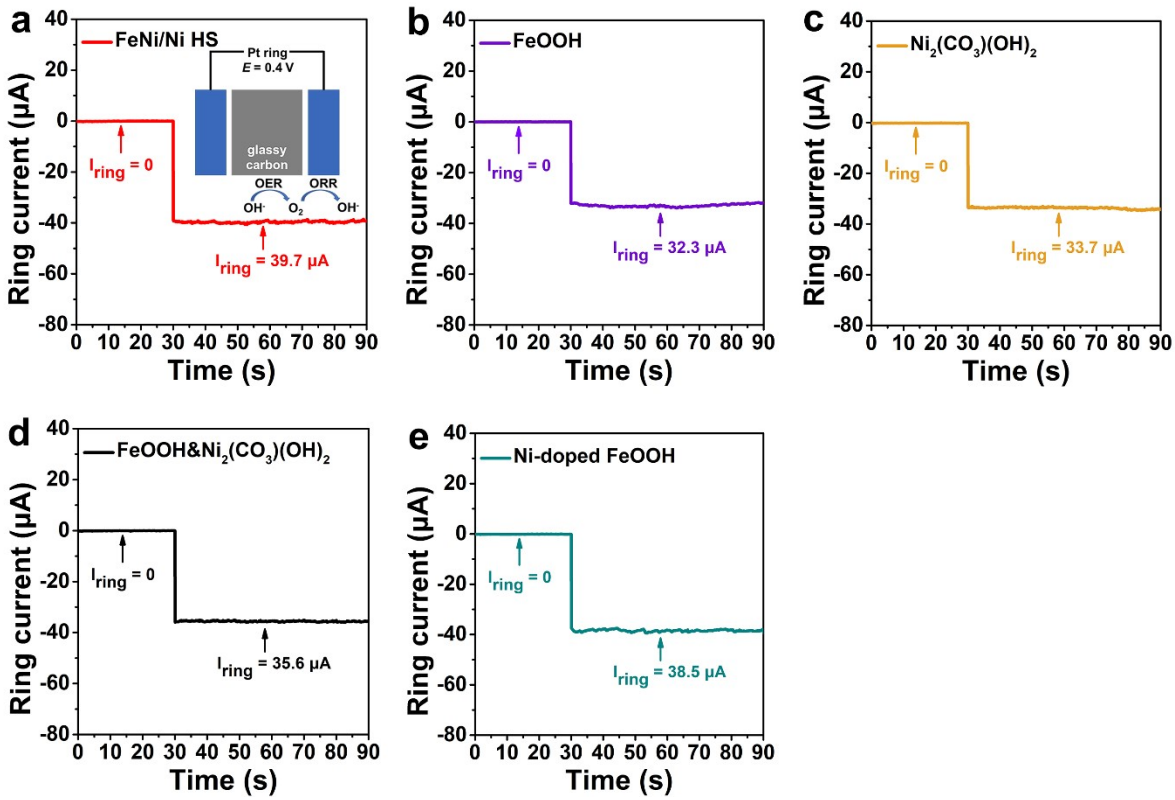

Fig. S11 Ring current measurements: (a) FeNi/Ni HS, (b) FeOOH, (c) $Ni_2(CO_3)(OH)_2$, (d) FeOOH&$Ni_2(CO_3)(OH)_2$, and (e) Ni-doped FeOOH, all being on an RRDE (1600 rpm) in N_2-saturated 1.0 M KOH solution (ring potential at 0.40 V *vs.* RHE).

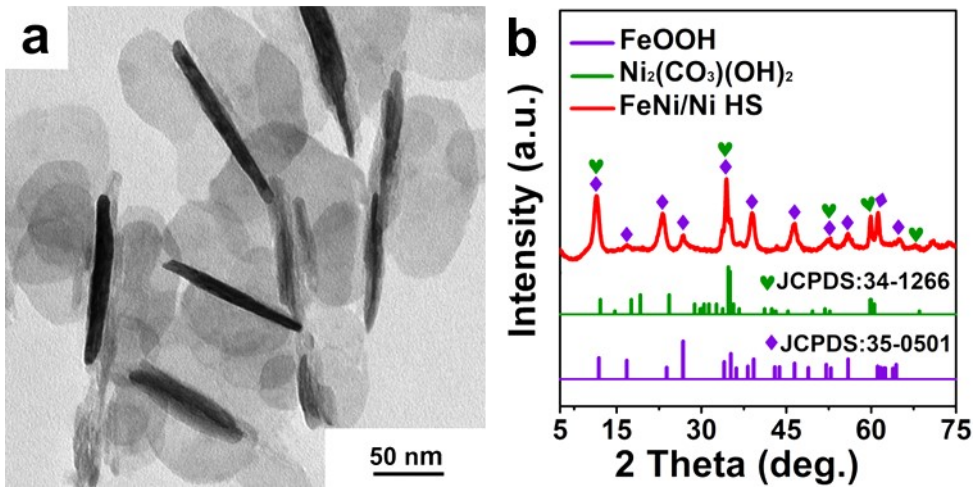

Fig. S12 Morphological and structural characterizations of FeNi/Ni HS recovered after the 40-h test. (a) TEM image. (b) XRD patterns.

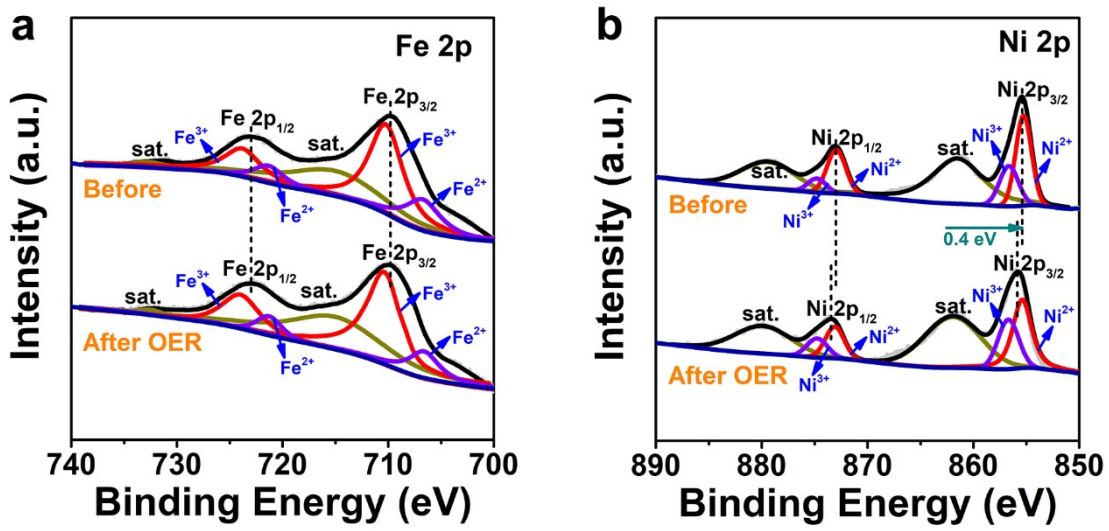

Fig. S13 XPS spectra of (a) Fe 2*p*, (b) Ni 2*p* for FeNi/Ni HS before and after the OER tests.

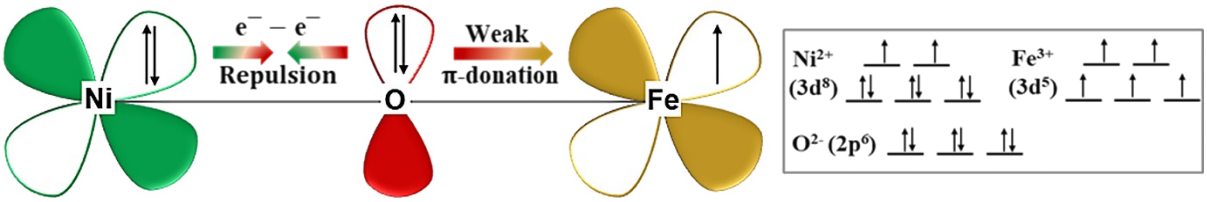

Fig. S14 Schematics of the electronic interplay between Ni and Fe via oxo bridge in FeNi/Ni HS.

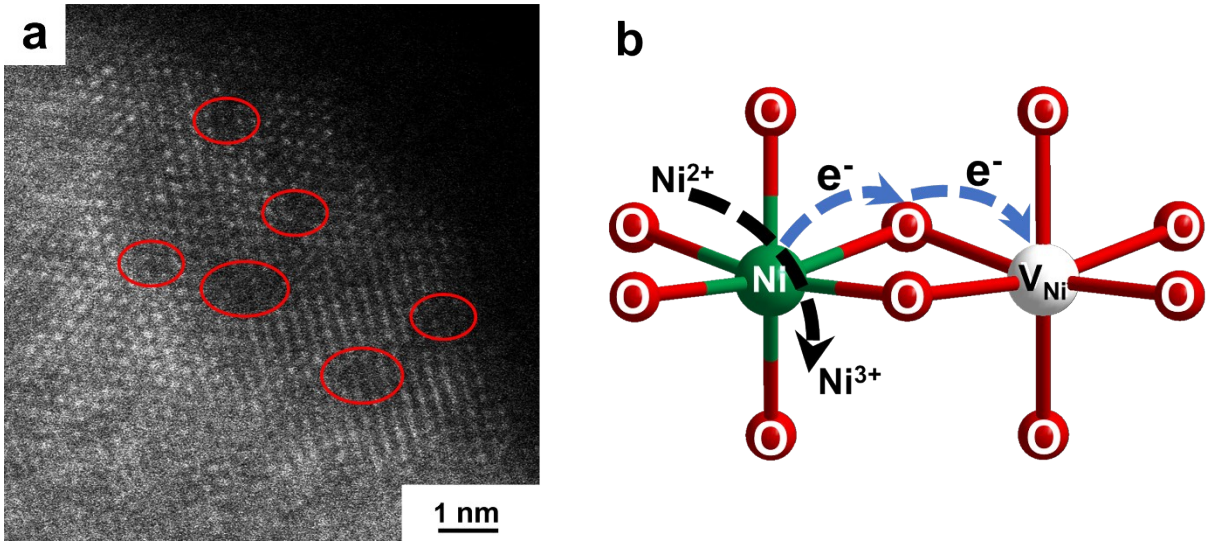

Fig. S15 The characterizations of Ni vacancies in the "wing" Region C. (a) HAADF-STEM image. (b) Electron transfer of Ni vacancies.

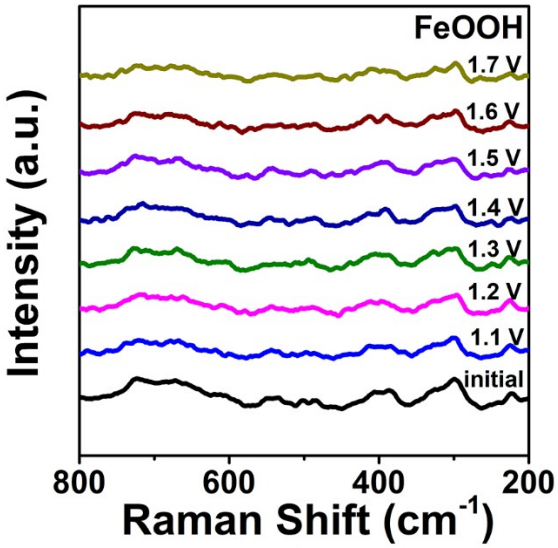

Fig. S16 *In-situ* Raman spectra of FeOOH at different voltages.

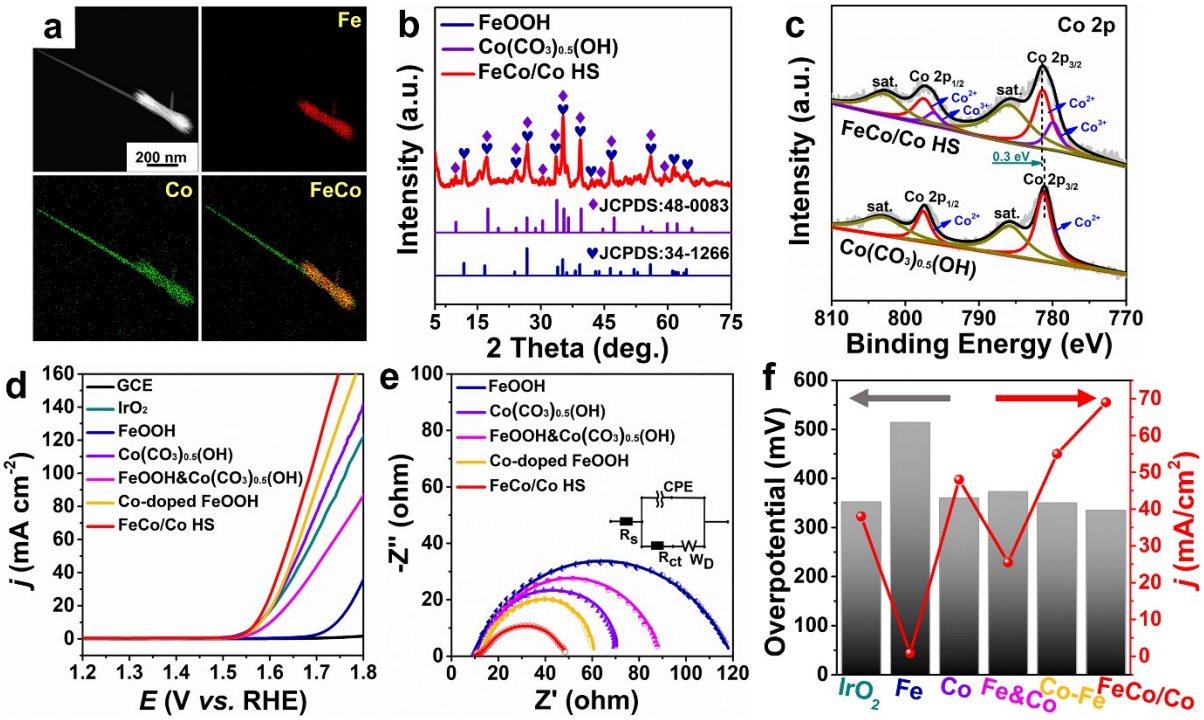

Fig. S17 Characterization and properties of FeCo/Co HS. (a) HAADF-STEM image and EDX elemental maps. (b) XRD patterns. (c) XPS spectrum of Co 2p. (d) Polarization curves. (e) Nyquist plots. (f) Overpotential at 10 mA cm^{-2} and current density at 1.65 V vs. RHE derived from the LSV curves.

The HAADF-STEM image (Fig. S17a) exhibited a saber-like structure, in which the hilt is about 400 nm length and 100 nm width, and the sword body is about 600 nm length and 20 nm width. EDX-mapping showed Co element throughout the structure, while Fe only in the hilt. XRD (Fig. S17b) confirmed the heterostructure consists of FeOOH (JCPDS: 34-1266) and $Co(CO_3)_{0.5}(OH)$ (JCPDS: 48-0083). The Co 2p XPS spectra (Fig. S17c) of FeCo/Co HS is fitted into two pairs of peaks, corresponding to Co^{2+} (781.2 eV, 797.5eV) and Co^{3+} (780.0eV, 796.3eV),[5,6] compare to $Co(CO_3)_{0.5}(OH)$, the binding energies of FeCo/Co HS exhibit positive shifts (0.3 eV), demonstrating in higher valence Co^{3+} in the heterostructures. LSV (Fig. S17d)

showed that the onset overpotential of FeCo/Co HS is 270 mV, which is the smallest in comparison groups. EIS (Fig. S17e) demonstrates that R_{ct} of FeCo/Co HS is also the smallest indicating superior charge transfer kinetics. Fig. S17f showed FeCo/Co HS exhibits the smallest overpotential and the largest current density, which again demonstrates its excellent catalytic activity.

Table S1. ICP analysis of FeNi/Ni HS with different metal ratios.

Catalysts	Ni (wt.%)	Fe (wt.%)	Ni/Fe
FeNi/Ni HS(Ni:Fe=1/1)	20.21	22.83	1.00/1.13
FeNi/Ni HS(Ni:Fe=3/2)	22.48	15.16	2.97/2.00
FeNi/Ni HS(Ni:Fe=2/1)	23.74	12.18	1.95/1.00

Table S2. Changes in metal content of FeNi/Ni HS over a course of 36 hours.

Time	Ni (wt.%)	Fe (wt.%)
3 h	19.84	80.16
6 h	38.97	61.03
18 h	50.97	49.03
36 h	61.14	38.96

Table S3. Comparisons of the electrocatalytic performance with reported catalysts.

Electrocatalyst	Medium	Oset potential (V *vs.* RHE)	Overpotential [a] (mV)	Stability [b] (h)	Reference
FeNi/Ni HS	1.0 M KOH	1.45	268	40	This work
Fe-CoOOH/G[7]	1.0 M KOH	1.51	330	5	*Adv. Energy Mater.* 2017, **7**, 1602148.
CoNi(OH)x[8]	1.0 M KOH	1.48	280	24	*Adv. Energy Mater.* 2016*,* **6***,* 150166.
α-$Co_4Fe(OH)_x$[9]	1.0 M KOH	1.48	295	3	*J. Mater. Chem. A,* 2017, **5**, 1078-1084.
NiCo LDH[10]	1.0 M KOH	1.53	367	6	*Nano Lett.* 2015, **15**, 1421-1427.
$NiCo_{2.7}(OH)_x$[11]	1.0 M KOH	1.48	350	10	*Adv. Energy Mater.* 2015, **5**, 1401880.
Fe-CoOOH/G[12]	1.0 M KOH	1.50	330	6	*Adv. Energy Mater.* 2017, **7**, 1602148.
FeOOH(Se)/IF[13]	1.0 M KOH	1.49	287	14	*J. Am. Chem. Soc.* 2019, **141**, 7005-7013*.*
$Co(OH)_2$@NCNTs@NF[14]	1.0 M KOH	1.40	270	200	*Nano Energy* 2018, **47**, 96-104.
Fe-CoNi LDH[15]	1.0 M KOH	1.45	260	12	*Appl. Surf. Sci.* 2021*,* **565***,* 150506*.*
NiCo LDH[16]	1.0 M KOH	1.40	264	25	*Nano Res.* 2022*,* **15***,* 4986-4995*.*
NiCo-LDH/$ZnCo_2O_4$[17]	1.0 M KOH	1.47	260	/	*J. Colloid Interface Sci.* 2021, **604**, 832-843.
$Fe_{0.33}Co_{0.67}OOH$ PNSAs/CFC[18]	1.0 M KOH	1.45	266	24	*Angew. Chem. Int. Ed*. 2018, **57**, 2672-2676.
ZNDP-1[19]	1.0 M KOH	1.30	170	/	*Appl. Surf. Sci.* 2021*,* **562***,* 150253*.*
NiFeV nanofibers[20]	1.0 M KOH	1.41	263	/	*Angew. Chem.Int. Ed.*

					2022*,* **61***, e2021153.*
Nb-NiFe-LDH[21]	1.0 M KOH	1.34	242	73 (100 mA cm^{-2})	*Chem. Eng. J.* 2022, **427**, 131643.
FeBi@FeNi LDH[22]	1.0 M KOH	1.47	246	90 (100 mA cm^{-2})	*J. Colloid Interface Sci.* 2022, **610**, 173-181.

[a] Overpotential at a current density of 10mA cm^{-2}; [b] Stability at a current density of 10 mA cm^{-2}.

3. Reference

1. X. H. Sun, Q. Shao, Y. C. Pi, J. Guo, X. Q. Huang, *J. Mater. Chem. A*, 2017, **5**, 7769.
2. D. Voiry, M. Chhowalla, Y. Gogotsi, N. A. Kotov, Y. Li, R. M. Penner, R. E. Schaak, P. S. Weiss, *ACS Nano* 2018, **12**, 9635-9638.
3. H. L. Fei, J. C. Dong, Y. X. Feng, C. S. Allen, C. Z. Wan, B. Volosskiy, M. F. Li, Z. P. Zhao, Y. L. Wang, H. T. Sun , P. F. An, W. X. Chen, Z. Y. Guo, C. Lee, D. L. Chen, I. Shakir, M. J. Liu, T. D. Hu, Y. D. Li, A. I. Kirkland, X. F. Duan, Y. Huang, *Nat. Catal.* 2018, **1**, 63.
4. T. Y. Ma, S. Dai, M. Jaroniec, S. Z. Qiao, *J. Am. Chem. Soc.* 2014, **136**, 13925.
5. L. Hui, Y. Xue, D. Jia, Yu, H.; Zhang, C.; Li, Y. *Adv. Energy Mater.* 2018, **8**, 1800175.
6. P. W. Menezes, S. Yao, R. Beltran-Suito, J. N. Hausmann, P. V. Menezes, M. Driess, *Angew. Chem. Int. Ed.* 2021, **60**, 4640-4647.
7. X. T. Han, C. Yu, S. Zhou, C. T. Zhao, H. W. Huang, J. Yang, Z. B. Liu, J. J. Zhao, J. S. Qiu, *Adv. Energy Mater*. 2017, **7**, 1602148.
8. S. W. Li, Y. C. Wang, S. J. Peng, L. J. Zhang, A. M. AI-Enizi, H. Zhang, X. H. Sun, G. F. Zheng, *Adv. Energy Mater*. 2016, **6**, 150166.
9. H. Y. Jin, S. J. Mao, G. P. Zhan, F. Xu, X. B. Bao, Y. Wang, *J. Mater. Chem. A*, 2017, **5**, 1078-1084.
10. H. F. Liang, F. Meng, M. C. Acevedo, L. S. Li, A. Forticaux, L. C. Xiu, Z. C. Wang, S. Jin, *Nano Lett.* 2015, **15**, 1421-1427.
11. J. W. Nai, H. J. Yin, T. T. You, L. R. Zheng, J. Zhang, P. X. Wang, Z. Jin, Y. Tian, J. Z. Liu, Z. Y. Tang, L. Guo, *Adv. Energy Mater.* 2015, **5**, 1401880.
12. X. Han, C. Yu, S. Zhou, C. Zhao, H. Huang, J. Yang, Z. Liu, J. Zhao, J. Qiu, *Adv. Energy Mater.* 2017, **7**, 1602148.
13. S. Niu, W. J. Jiang, Z. X. Wei, T. Tang, J. M. Ma, J. S. Hu, L. J. Wan, *J. Am. Chem. Soc.* 2019, **141**, 7005-7013.
14. P. Guo, J. Wu, X. B. Li, J. Luo, W. M. Lau, H. Liu, X. L. Sun, L. M. Liu, *Nano Energy* 2018, **47**, 96-104.
15. Y. L. Shi, J. Q. Li, B. Y. Zhang, S. Y. Lv, T. Wang, X. Liu, *Appl. Surf. Sci.* 2021*,* **565***,* 150506*.*

16. J. H. Li, L. L. Wang, H. J. He, Y. Q. Chen, Z. R. Gao, N. Ma, B. Wang, L. L. Zheng, R. L. Li, Y. J. Wei, J. Q. Xu, Y. Xu, B. W. Cheng, Z. Yin, D. Ma, *Nano Res.* 2022*,* **15***,* 4986-4995*.*
17. M. Shamloofard, S. Shahrokhian, M. K. Amini, *J. Colloid Interface Sci.* 2021, **604**, 832-843.
18. S. H. Ye, Z. X. Shi, J. X. Feng, Y. X. Tong, G. R. Li, *Angew. Chem. Int. Ed*. 2018, **57**, 2672-2676.
19. J. Jana, K. C. Bhamu, Y. T. Ngo, S. G. Kang, J. S. Chuang, *Appl. Surf. Sci.* 2021*,* **562***,* 150253*.*
20. B. Zhang, Z. H. Wu, W. J. Shao, Y. Gao, W. W. Wang, T. Ma, L. Ma, S. Li, C. Cheng, C. S. Zhao, *Angew. Chem.Int. Ed*. 2022, **61**, e2021153.
21. Y. N. Zhou, F. L. Wang, S. Y. Dou, Z. N. Shi, B. Dong, *Chem. Eng. J.* 2022, **427**, 131643.
22. F. G. Wang, B. Liu, H. Y. Wang, Z. Y. Lin, Y. W. Dong, N. Yu, R. N. Luan, Y. M. Chai, B. Dong, *J. Colloid Interface Sci.* 2022, **610**, 173-181.